

Computing White Matter Fiber Orientations in High Angular Resolution Diffusion-Weighted MRI

Ning Cao*, Qi Zhuang*, Xuwei Liang*, Ruiwang Huang[◇] and Jun Zhang*
 University of Kentucky*
 Lexington, KY 40506-0046, U.S.A.

IME Research Center[◇]
 Juelich, Germany

Abstract

Diffusion tensor magnetic resonance imaging (DTI) can resolve white matter fiber orientations within voxels in which the diffusion is characterized by Gaussian diffusion process. High angular resolution diffusion imaging (HARDI) adds the capability of describing the apparent diffusion coefficient (ADC) profile of voxels that contain kissing, branching and crossing fiber configurations. We present a new method for recovering BiGaussian model from HARDI. This method divides the parameters of biGaussian model into the parameters describing the shape of ADC profile and the parameters defining the orientation of ADC profile. The two types of parameters are recovered in separate steps.

Keywords: high angular resolution diffusion imaging (HARDI), apparent diffusion coefficient (ADC), BiGaussian, tractography.

1. Introduction

Medical imaging techniques have achieved vital importance in providing visual and quantitative information for diagnosing disease or abnormality. Diffusion-weighted magnetic resonance imaging (DWI) of the brain has become popular in the past few years because of its capability to provide both local anisotropy and global structural connectivity information within the white matters. Diffusion-weighted signal $S(g)$ along different gradients g and the unweighted signal S_0 are measured using some b value for each voxel. The ADC profile $d(\theta, \phi)$ is defined as

$$S(g) = S_0 e^{-bd(\theta, \phi)} \quad (1)$$

where g is a unit vector

$$g = \begin{pmatrix} x \\ y \\ z \end{pmatrix} = \begin{pmatrix} \sin \theta \cos \phi \\ \sin \theta \sin \phi \\ \cos \theta \end{pmatrix}$$

The angles θ and ϕ ($0 \leq \theta \leq \pi, 0 \leq \phi \leq 2\pi$) represent the polar angle from the z-axis and azimuthal angle in the x y -plane.

The ADC profile defined in (1) can be visualized by a peanut-like parameter surface defined by spherical coordinate

$\rho(\theta, \phi) = d(\theta, \phi)$ [1] [2] [3], by coloring a sphere according to $d(\theta, \phi)$, or by both [4] [5] [6]. Although the ADC profile is always shown as a surface in a 3D space, it is defined on the 2-sphere.

The diffusion tensor model proposed by Basser et al. [7] assumes the diffusion to be Gaussian, thus the ADC profile can be described by a single second order tensor D . Fiber tractography on fiber bundles with high anisotropy works well but the Gaussian assumption tends to fail in the regions with multiple fibers crossing or kissing [8]. Tuch et al. [2] proposed to use HARDI which measures diffusion-weighted signals at many gradient directions to better measure the ADC profile.

In order to better describe the diffusion profile, Frank et al. used spherical harmonics (SH) [9] [10] truncated to a certain order to approximate the ADC profile [6] to get a continuous function on the unit sphere. Ozarslan et al. [3] fit the ADC profile using High Order Diffusion Tensor (HODT). Descoteaux et al. proposed to use the real spherical harmonics [11] which is a linear combination of the spherical harmonics functions and proved that the HODT basis functions can also be obtained from spherical harmonics functions [5].

White matter fiber tracking algorithms [12] [13] use local fiber directions to provide fiber pathways *in vivo*. Although deriving fiber directions from diffusion tensor model is straightforward [14] [15], obtaining the correct fiber directions from various HARDI models is more challenging. The maxima of the ADC profile do not agree with fiber directions generally [5]. In addition to using SH to describe the ADC profile, different diffusion models have been introduced recently, e.g., the finite Gaussian mixture is [2]

$$S(g_i) = S_0 \sum_{k=1}^N f_k e^{-bg_i^T D_k g_i} \quad (2)$$

where $\sum k = 1$.

The biGaussian model is a special case of (2) with $N = 2$. To reduce the number of unknown parameters of (2), eigenvalues of D_1 and D_2 are assumed to represent normal values [16] [2], with $\lambda_1 \geq \lambda_2 = \lambda_3$. Therefore the number of free parameters is reduced from 13 to 5. In order to derive the fiber directions of the biGaussian model, different optimization methods [2] have been used and some of them [2] require multiple restarts.

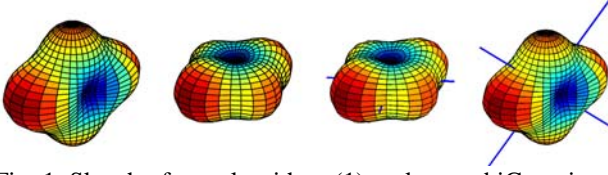


Fig. 1. Sketch of our algorithm. (1): unknown biGaussian ADC profile to be recovered. (2): the unknown ADC profile was rotated according to moment of inertia tensor to make its principle axes align with coordinate axes. (3): the best matched template was found with known fiber directions. (4): getting fiber directions of the original unknown ADC profile by rotating the template.

This paper provides an easy method to estimate the fiber directions of the biGaussian model using moment and moment of inertia tensor.

2. Theory

The surface defined by ADC profile $d(\theta, \phi)$ can be regarded as a rigid object in 3D space. For a rigid object of N points, the moment of the rigid object can be defined as

$$M_{pqr} = \sum_{i=1}^N m_i x_i^p y_i^q z_i^r \quad (3)$$

and the moment of inertia tensor is defined as [17]

$$I = \begin{pmatrix} I_{xx} & I_{xy} & I_{xz} \\ I_{yx} & I_{yy} & I_{yz} \\ I_{zx} & I_{zy} & I_{zz} \end{pmatrix} \quad (4)$$

where

$$\begin{aligned} I_{xx} &= \sum_{i=1}^N m_i (y_i^2 + z_i^2), \\ I_{yy} &= \sum_{i=1}^N m_i (x_i^2 + z_i^2), \\ I_{zz} &= \sum_{i=1}^N m_i (x_i^2 + y_i^2), \\ I_{xy} = I_{yx} &= -\sum_{i=1}^N m_i x_i y_i^2, \\ I_{xz} = I_{zx} &= -\sum_{i=1}^N m_i x_i^2 z_i^2, \end{aligned}$$

and

$$I_{yz} = I_{zy} = -\sum_{i=1}^N m_i y_i^2 z_i^2.$$

The eigenvalues (I_1, I_2, I_3) of the moment of inertia tensor (4) are called the principal moments of inertia and the eigenvectors are called principal axes. If two principal moments are equal, the rigid object is called a symmetrical top and the choice for the two corresponding principal axes is arbitrary.

3. Method

Different values of the parameters of biGaussian model lead to different shapes of the ADC profile. The shape of an ADC profile may be a peanut (Fig. 2 right), a star (Fig. 2 left),

or some shapes between them. The shape of the ADC profile is decided by the eigenvalues λ_i of the two tensors, the volume ratio f , the angle between the two tensors α and the b value. Two ADC profiles having the same shape only differ up to a rotation. Parameters other than λ_i , f , α and b decide the orientation of the ADC profile.

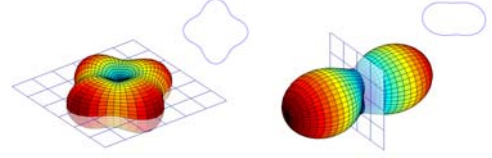


Fig. 2. Two types of symmetrical tops and sections (upper right) vertical to their principal axes. Left: $I_1 \approx I_2 \gg I_3$ and α is around 90° ; right: $I_1 \gg I_2 \approx I_3$ when α is small. The shape of the section is used to align the ADC profile to coordinate axis.

While most optimization methods try to find all the parameters of the biGaussian model at once, our method recovers the parameters in two steps. The parameters describing the shape of the unknown ADC profile are decided by matching the unknown ADC profile to precalculated templates of ADC profiles having similar shapes, then the direction information is recovered by rotating the matched template to the unknown ADC profile.

3.1. Algorithm

A template table contains moments as well as direction information of the templates is built before processing the biGaussian model in each voxel. Each entry of the table represents the combination of different f and α , while the eigenvalues λ_i and b value are considered as constants of a particular scan.

To find a configuration best match the measured diffusion profile, we take the following steps for each voxel (Fig. 1):

- 1) The moment of inertia tensor I is computed using (4), and the eigenvectors of I are sorted in ascending order according to their corresponding eigenvalues to form a rotation matrix V . Then, the unknown biGaussian profile is rotated by using

$$\hat{g} = V^T g \quad (5)$$

to make the principal axes align with coordinate axes. If the profile is a symmetrical top, it is possible that only the unique principal axis is aligned.

- 2) Several orders of moment are calculated using \hat{g} and $S(\hat{g}) = S(g)$ (also $-\hat{g}$ and $S(\hat{g})$) by (3) as

$$M_{pqr} = \sum_{i=1}^N \omega_i \hat{x}_i^p \hat{y}_i^q \hat{z}_i^r S(g_i), \text{ where } \omega_i \text{ is the weight of}$$

each measurement, \hat{x}_i , \hat{y}_i and \hat{z}_i are the elements of vector \hat{g} . In this paper, the weight is set to 1. The moments are then used to find the best matched template in the precalculated template table.

- 3) If the unknown ADC profile is a symmetrical top, the shape of the section vertical to its principal axis is used to further align the profile to coordinate axes (Fig. 2). The other two columns of V are fixed in this step.
- 4) At last, the two fiber directions of the template are rotated back by V to get fiber directions of the unknown ADC profile.

Six moments of even order (2, 0, 0), (0, 2, 0), (2, 2, 0), (1, 3, 0), (3, 1, 0) and (3, 3, 0) are chosen in our test. The orders of \hat{z}_i are set to 0 because most information is provided by \hat{x}_i and \hat{y}_i after the ADC profile is rotated by (5).

3.2. Simulation

To evaluate the performance of our method, synthetic data were generated using the biGaussian model.

- 1) 30 gradient directions were chosen in the simulation.
- 2) Orientations of the two fibers were represented by random rotation matrices R_1, R_2 and volume ratio $f = 0.5$.
- 3) The two fibers were defined by diffusion tensor D_1 and D_2 , where $D_k = R_k^T \Lambda R_k$, and matrix Λ is the eigenvalues, set to (1.7, 0.3, 0.3) $\mu m^2/ms$. The biGaussian ADC profile was generated using (2) with $N = 2$ and $b = 1000$.
- 4) Rician noise was added to $S(g_i)$ and S_0 . Gaussian noise was added to both the real part and the imaginary part of the complex signal. The signal-to-noise ratio (SNR) of S_0 was set to 65 and that of $S(g_i)$ was set to 25, 35 and 45.

3.3. Data Acquisition and Processing

Approval for this study was received from the IME Research Center Internal Review Board, Juelich, Germany. Diffusion image of a healthy adult male was taken at 2T (GE Signa), $b = 1000 s/mm^2$, and $2.0 \times 2.0 \times 2.0 mm^3$. The weighted images were obtained from 30 gradient directions and the unweighted images were scanned 6 times. SNR was around 65 in the unweighted image and around 35 in the weighted images.

In order to eliminate motion artifacts, the unweighted images were registered to the first unweighted image to get an averaged S_0 image. Diffusion-weighted images were

registered to the averaged unweighted image to remove artifacts introduced by motion and Eddy current effect [18].

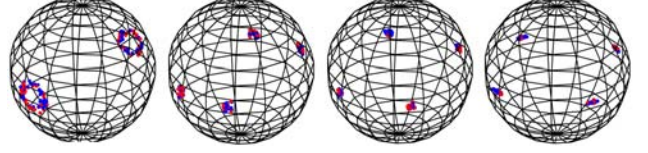


Fig. 3. Accuracy of the fitting: simulation samples of $\alpha = 20^\circ$, $\alpha = 40^\circ$, $\alpha = 60^\circ$ and $\alpha = 80^\circ$. Fitting results of fiber orientations are shown as points on the unit spheres, with each point representing a vector. Sixty trials were performed for each α , SNR=35/65 for weighted/unweighted images and $b = 1000$.

Currently, no model selection was performed in this work. The diffusion tensor model was covered by the biGaussian model with the angle α set to 0.

4. Results

The accuracy of the biGaussian model can be measured by error of volume ratio, error of angle between the two tensors $\alpha_{err} = |\alpha - \hat{\alpha}|$ and average minimum angle θ_{err} defined by Tuch et al. [2] (Fig. 4).

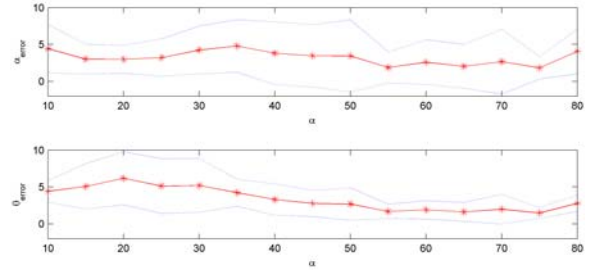


Fig. 4. Fitting errors (mean \pm SD) of the simulation. α_{err} and θ_{err} are plotted as a function of the angle α . Sixty trials were performed for each α , SNR=35/65 for weighted/unweighted images and $b = 1000$. All angles are in degree.

The volume ratio and the angle α were always recovered with high accuracy when the ADC profile was not a symmetrical top. It seemed that SNR did not affect the fitting results very much.

Several regions of interest (ROIs) are selected in the human brain to test the biGaussian fitting and one of the results is shown in (Fig. 5). Please note that some ADC profiles are too complex for the biGaussian model.

5. Discussion and Conclusion

With a few assumptions, the method reported here may recover the biGaussian model from ADC profiles with good accuracy. The calculation is simple and does not need multiply restarts.

Our simulations show that the θ_{err} is not large when the angle α is small, i.e., $\alpha < 45^\circ$ (Fig. 4), and this also can be seen in [2]. But we do not recommend to use the biGaussian model when α is small because the biGaussian model does not provide more information than the diffusion tensor model in this situation.

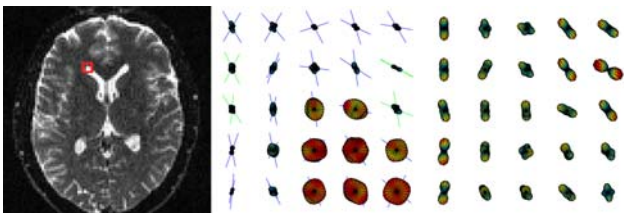


Fig. 5. Fitting results of human brain data. Left: ROI defined on the unweighted image. Middle: ADC profile and fiber orientations derived by our method. Right: recovered biGaussian ADC profile.

Recovering fiber orientations from the biGaussian model is an optimization problem. Fiber tracking algorithms always require high accuracy fiber orientations to produce reliable fiber tracks. With the current low accuracy of fiber orientations from HARDI, the level of confidence of the fitting result should be considered by the tracking algorithms when fiber pathways are determined.

The biGaussian model is better than the diffusion tensor model because it can describe more complex diffusion profiles. But we found that there are some voxels that the biGaussian model is inadequate.

More work is needed for the validation of the biGaussian model as well as other diffusion models to describe the diffusion process of interested regions within the human brain. The verification of the fiber orientations derived from various diffusion models is also a challenging job.

Acknowledgment

This work was supported in part by the U.S. National Science Foundation under grant CCF-0527967, in part by the Kentucky Science and Engineering Foundation under grant KSEF-148-502-06-186, and in part by Alzheimer's Association under grant NIGR-06-25460.

Citation Source: Technical Report TR 481-07, Department of Computer Science, University of Kentucky, Lexington, KY, 2007.

References

- [1] D. Alexander, G. Barker, and S. Arridge, "Detection and modeling of non-Gaussian apparent diffusion coefficient profiles in human brain data," *Magnetic Resonance in Medicine*, vol. 48, no. 2, pp. 331–340, 2002.
- [2] D. Tuch, T. Reese, M. Wiegell, N. Makris, J. Belliveau, and V. Wedeen, "High angular resolution diffusion imaging reveals intravoxel white matter fiber heterogeneity," *Magnetic Resonance in Medicine*, vol. 48, no. 4, pp. 577–582, 2002.
- [3] E. Oezarslan and T. Mareci, "Generalized diffusion tensor imaging and analytical relationships between diffusion tensor imaging and high angular resolution diffusion imaging," *Magnetic Resonance in Medicine*, vol. 50, no. 5, pp. 955–965, 2003.
- [4] L. Frank, "Anisotropy in high angular resolution diffusion-weighted MRI," *Magnetic Resonance in Medicine*, vol. 45, no. 6, pp. 935–939, 2001.
- [5] M. Descoteaux, E. Angelino, S. Fitzgibbons, and R. Deriche, "Apparent diffusion coefficients from high angular resolution diffusion imaging: Estimation and applications," *Magnetic Resonance in Medicine*, vol. 56, pp. 395–410, 2006.
- [6] L. Frank, "Characterization of anisotropy in high angular resolution diffusion-weighted MRI," *Magnetic Resonance in Medicine*, vol. 47, no. 6, pp. 1083–1099, 2002.
- [7] P. Basser, J. Mattiello, and D. LeBihan, "MR diffusion tensor spectroscopy and imaging," *Biophysical Journal*, vol. 66, no. 1, pp. 259–267, 1994.
- [8] D. Tuch, R. Weisskoff, J. Belliveau, and V. Wedeen, "High angular resolution diffusion imaging of the human brain," *Proceedings of the 7th Annual Meeting of ISMRM*, 1999.
- [9] W. Byerly, *An Elementary Treatise on Fourier's Series and Spherical, Cylindrical, and Ellipsoidal Harmonics. With Applications to Problems in Mathematical Physics*. Adamant Media Corporation.
- [10] T. MacRobert, *Spherical Harmonics: An Elementary Treatise on Harmonic Functions with Applications*. Pergamon Press, 1967.
- [11] R. Martin, *Electronic Structure: basic theory and practical methods*. Cambridge University Press, 2004.
- [12] S. Mori, B. Crain, V. Chacko, and P. van Zijl, "Three-dimensional tracking of axonal projections in the brain by magnetic resonance imaging," *Ann Neurol*, vol. 45, no. 2, pp. 265–9, 1999.
- [13] N. Kang, J. Zhang, E. Carlson, and D. Gembris, "White matter fiber tractography via anisotropic diffusion simulation in the human brain," *IEEE Transactions on Medical Imaging*, vol. 24, no. 9, pp. 1127–1137, 2005.
- [14] P. Basser, "Fiber-tractography via diffusion tensor MRI (DT-MRI)," *Proceedings of International Society for Magnetic Resonance in Medicine*, vol. 1226, 1998.
- [15] S. Mori, B. Crain, and P. van Zijl, "3D brain fiber reconstruction from diffusion MRI," *Proceedings of International Conference on Functional Mapping of the Human Brain*, 1998.
- [16] C. Pierpaoli, P. Jezzard, P. Basser, A. Barnett, and G. Di Chiro, "Diffusion tensor MR imaging of the human brain," *Radiology*, vol. 201, no. 3, pp. 637–48, 1996.

[17] H. Goldstein, C. Poole, J. Safko, and S. Addison, "Classical Mechanics," *American Journal of Physics*, vol. 70, p. 782, 2002.

[18] R. Nunes, I. Drobnjak, S. Clare, P. Jezzard, and M. Jenkinson, "Quantitative simulation of affine registration for correction of eddy current distortions in diffusion-weighted images." *Proceedings of International Society for Magnetic Resonance in Medicine*, 2005.